Chemical Physics Letters 512 (2011) 76–80

Contents lists available at ScienceDirect

Chemical Physics Letters

journal homepage: www.elsevier.com/locate/cplett

Probing nanoscopic droplet interfaces in aqueous solution with vibrational sum-frequency scattering: A study of the effects of path length, droplet density and pulse energy

Hilton B. de Aguiar, Jean-Sebastien Samson, Sylvie Roke *

Laboratory for fundamental BioPhotonics (LBP), Institute of Bioengineering (IBI), School of Engineering (STI), École Polytechnique Fédérale de Lausanne (EPFL), 1015 Lausanne, Switzerland
Max-Planck Institute for Intelligent Systems, 70569 Stuttgart, Germany

ARTICLE INFO

Article history:
Received 24 March 2011
In final form 26 June 2011
Available online 1 July 2011

ABSTRACT

We present a description of sum frequency scattering experiments to probe the interfacial vibrational spectrum of nanoscopic oil droplets dispersed in water. SF scattering measurements as a function of optical path length, infrared (IR) pulse energy and particle density show that for different IR excitation wavelengths a different optimum experimental geometry exists. The optimum optical path length matches roughly the 1/e absorbance length in D_2O of the used IR frequency. The intensity depends linearly on the particle density. The SF intensity also scales linearly with the IR pulse energy, whereas no changes are observed in the spectral shape.

1. Introduction

Interfacial properties can determine the macroscopic properties of dispersions consisting of sub-micron sized particles or droplets [1,2]. Ionic surfactants adsorbed at the droplet/oil interface can influence the stability of droplets in emulsions and chemically crafted polymers or alkanes can stabilize particles by means of steric stabilization [3]. Although such processes are well understood on the macroscopic scale the study of molecular properties of droplet or particle interfaces in solution is a challenge because it is difficult to distinguish bulk molecules from surface molecules. A probe also needs to penetrate the liquid phase, which is not always transparent. Furthermore, small particles undergo Brownian motion and scatter light.

Second-Harmonic Scattering (SHS) and vibrational Sum-Frequency Scattering (SFS) are recently developed Nonlinear Light Scattering (NLS) techniques, capable of selectively probing the interfaces of particles or droplets in a dispersion [4,5]. SHS has been pioneered by the Eisenthal group and has been applied to study a number of colloidal phenomena such as electrostatic properties of polymer particle surfaces [6,7], adsorption of molecules at colloidal interfaces [8–11], surface acid-basic equilibria [12] and molecular transport across liposome bilayers [13,14] with SHS. Sum frequency scattering offers additional chemical specificity, since it allows to probe the vibrational spectrum of molecules on the particle/solution interface [15]. SFS has been used to probe colloidal phase transitions [16,17] in apolar solvents, crystalline domains in amorphous polymer microspheres [18], adsorption of surfactants at oil droplets dispersed in water [19,20] and asymmetry in catanionic vesicles dispersed in water [21].

Here, we show details of the implementation of the SF scattering experiment to study oil droplets in water. We first introduce the background for the SFS technique and also discuss other light/matter processes that occur in a dispersion, such as absorption and linear scattering. A detailed description of the experiment is followed by experiments aimed to describe in detail various aspects of sum frequency scattering. We performed SF scattering measurements on emulsions consisting of ~100 nm sized oil droplets dispersed in SDS/D_2O solutions. We report SF scattering measurements as a function of optical path length, pulse energy and particle density.

2. Sum frequency scattering background

In an SFS experiment, mid-infrared (IR) and visible (VIS) pulsed laser beams are overlapped inside a cuvette containing dispersed particles in a liquid or solid matrix [16,18]. Figure 1A illustrates the process and the important parameters. At the particle interface, a second-order nonlinear polarization is created which oscillates at the sum of the IR and VIS frequencies. This polarization is small but does not vanish because there is a phase difference between the polarization components generated on different parts of the sphere. The SF photons generated at the surface coherently interfere at the detector position and generate a scattering pattern.

* Corresponding author. Addresses: Laboratory for fundamental BioPhotonics (LBP), EPFL-STI-IBI-LBP, Station 17, CH-1015 Lausanne, Switzerland, Max-Planck Institute for Intelligent Systems, Spectroscopy at Bio-interfaces, Heisenbergstrasse 3, D-70569 Stuttgart, Germany. Fax: +49 711 6893612.
E-mail addresses: sylvie.roke@epfl.ch, roke@mf.mpg.de (S. Roke).

0009-2614/$ - see front matter © 2011 Elsevier B.V. All rights reserved.
doi:10.1016/j.cplett.2011.06.081

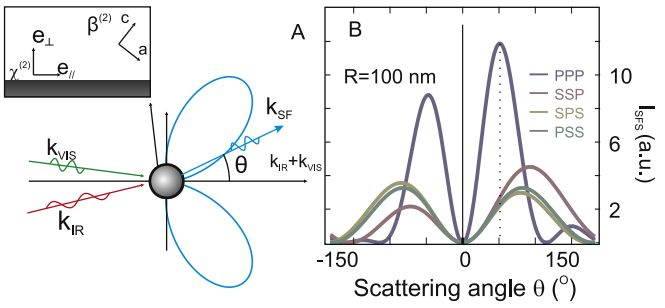

Figure 1. Sum frequency scattering. (A) Important parameters for the sum frequency scattering experiment. The $\chi^{(2)}$ components are defined as perpendicular ($\perp$) or parallel ($\parallel$) to the droplet interface. All beams lie in the horizontal plane. (B) Scattering pattern for a droplet with a 100 nm radius (R) in different polarization combinations, assuming that $\boldsymbol{\chi}^{(2)} = 0$, except $\boldsymbol{\chi}^{(2)}_{\perp\perp\perp} = 1$.

The scattering pattern depends on droplet size, experimental geometry and surface structure [22,23,11,24].

The SFS spectrum detected at an angle θ from a single particle can be described by the following equation:

$$I_{SF}(\theta, R, \omega) \propto \frac{k_0^4}{r_0^2} |\boldsymbol{\Gamma}^{(2)}(\theta, R, \omega)|^2 I_{IR} I_{VIS} \tag{1}$$

$$\boldsymbol{\Gamma}^{(2)}(\theta, R, \omega) \propto N_s G\left(F_1(\theta, R), F_2(\theta, R), \boldsymbol{\chi}^{(2)}(\omega)\right)$$

The scattered intensity depends on the distance between the particle and the detector (r_0), the scattered wave vector ($\mathbf{k}_0$), the (local) intensity of the IR (I_{IR}) and VIS (I_{VIS}) beams, and on the effective particle susceptibility $\boldsymbol{\Gamma}^{(2)}$. The magnitude of $\boldsymbol{\Gamma}^{(2)}$ depends on a function G that contains the nonlinear optical surface response ($\boldsymbol{\chi}^{(2)}$), scattering geometry, particle size (R) and the surface density of vibrational groups (N_s). The angular direction of the peak intensity depends on the scattering form factor functions F_1 and F_2, which can be found in Ref. [25]. $\boldsymbol{\Gamma}^{(2)}$ also depends on the second order surface susceptibility ($\boldsymbol{\chi}^{(2)}(\omega)$) elements. $\boldsymbol{\chi}^{(2)}(\omega)$ is the product of the IR and Raman tensor components averaged over all surface molecular orientations on the droplet.

2.1. Angular distribution of the SFS process

The angular direction in which the SFS intensity is peaked changes with particle size [22,26,9,27,25,11,24]. Therefore, knowledge of the particle size distribution in the sample is key to a successful experiment. Once the particle size distribution is known, the position of the detection system can be chosen, whereby we use a calculated scattering pattern for the particular size distribution as a guide to determine the optimal detection angle. As the detection system consist of optics in combination with an I-CCD camera mounted on a spectrograph it is impractical to optimize the signal by scanning through a range of scattering angles.

Figure 1B shows a scattering pattern of a particle with a radius of 100 nm, for different polarization combinations, using the same Rayleigh–Gans–Debye formalism as described in Ref. [25]. *p* refers to beams polarized parallel to the plane of the incoming VIS and IR beams and *s* refers to a polarization direction perpendicular to that. It can be seen that different polarization combinations are peaked at different scattering angles. For all polarization combinations, however, the signal vanishes in the forward direction. for particles with a bulk refractive index close to the bulk refractive index of the surrounding medium and a size $R < 200$ nm, the size dependence of the scattered intensity per particle is: $I_{SF} \propto R^6$ [27]. For n particles the intensity of each particle needs to be added. If we have a constant IR and VIS field through the overlap volume and no correlations between the particles, this will result in a total signal (S_{SF}) of:

$$S_{SF} = \sum_{i=0}^{n} I_{SF,i} = n I_{SF} \propto \phi R^3 \tag{2}$$

for spherical particles with ϕ the volume fraction of the sample. As the sample consists of particles in solution, linear light scattering effects of the incoming beams and extinction of the incoming fields due to absorption may also play a role. This effect is described next.

2.2. Effects of optical path length and liquid medium on the generated signal

The intensity of the IR and VIS beams will vary along the optical axis due to absorption and/or scattering processes. If D_2O is used as bulk liquid, the IR beam is attenuated by absorption. Figure 2 shows IR transmission spectra for optical path lengths of 25, 200, and 1000 μm. It can be seen that 1 mm of D_2O is optically closed for a major portion of the infrared spectrum. Also, different absorption cross-sections exist for different wavelengths. For the vibrational modes studied here, the C–H modes, which vibrate around 2900 cm^{-1}, and the S–O stretch mode, which vibrates around 1070 cm^{-1}, the 1/e extinction lengths are 145 and 30 μm, respectively. As well as linear scattering, this can influence the optical layout of the SFS experiment.

As D_2O is transparent for visible light, attenuation of the VIS beam is mainly due to linear scattering. The IR and VIS beams therefore have a different dependence on optical path length. This different transmission dependence is illustrated in Figure 2B, which shows a sketch of the IR and VIS beam intensities in the transmitted direction as a function of propagation distance. If there is a cuvette with length d, and an optical axis z we need to take into account that the IR, and the VIS beam are changing along the optical axis (along ($\mathbf{k}_0$)). We thus have for the signal S (d):

$$\begin{aligned} I_{IR}(z) &\propto e^{-\alpha_{IR} A z} e^{-\tau_{IR} A \rho z} I_{IR,0}, \\ I_{VIS}(z) &\propto e^{-\tau_{VIS} A \rho z} I_{VIS,0}, \\ S_{SFS,tot}(d) &\propto \int_0^d dz \left|\Gamma^{(2)}\right|^2 I_{VIS}(z) I_{IR}(z) A \rho \end{aligned} \tag{3}$$

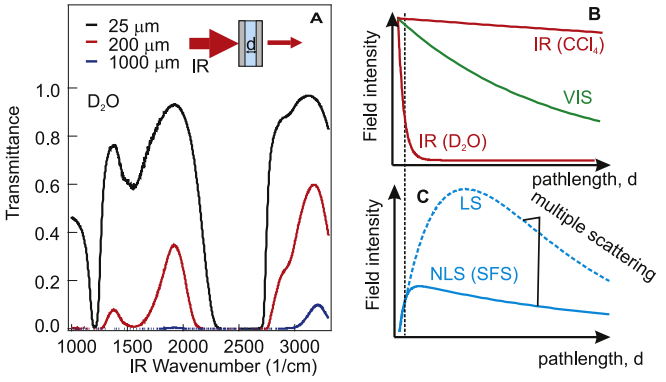

Figure 2. IR absorption, linear scattering (LS) and nonlinear light scattering (NLS) processes. (A) IR transmission spectra through a CaF_2 cuvette with varying path length, containing D_2O. (B) Sketch of the spatial intensity dependence of the exciting IR and VIS beams for IR transparent media and IR absorbing media (such as water). (C) Sketch of expected intensity dependence on the optical path length in the case that (1) IR absorption by the bulk medium is the limiting process (NLS), or (2) light scattering processes are the limiting factors (LS). The overall SFS intensity continuously increases with sample cell path length due to incoherent addition of radiation from separate droplets. The added signal from probing a larger volume levels off as a consequence of extinction of the incoming beams. This extinction occurs due to absorption of IR or VIS light by the medium, or linear light scattering in the sample. The signal intensity is further reduced due to multiple scattering events.

where α_{IR} is the absorption coefficient of the IR beam, τ_{IR} (τ_{VIS}) the extinction of the IR (VIS) beam due to scattering, A the overlap area, ρ the particle density, and I_0 the incoming intensity. As both IR and VIS beams travel through the suspension, they lose intensity due to linear scattering and absorbance. The amount of generated SF light will therefore not be uniform across the overlap volume.

The formulas in the above equations will give rise to a curve that grows in intensity with path length up to a certain point after which it stays constant. In reality, the intensity will decrease with path length because of multiple scattering. Multiple scattering includes the additional linear scattering of the SF photons, the VIS and IR photons. The resulting behavior will be an exponential decay. A precise description of these processes is mathematically complex and in general, multiple and correlated light scattering and the combined effect thereof is difficult to describe [28]. In general, if the path length or the particle density increases beyond the regime of single scattering, the total scattering intensity will decrease exponentially as illustrated in Figure 2C. For this behavior, path length and particle density are equivalent. Figure 2C also shows a comparison for linear light scattering of e.g. the VIS pulse and nonlinear light scattering of SF photons generated in a dispersion in D_2O.

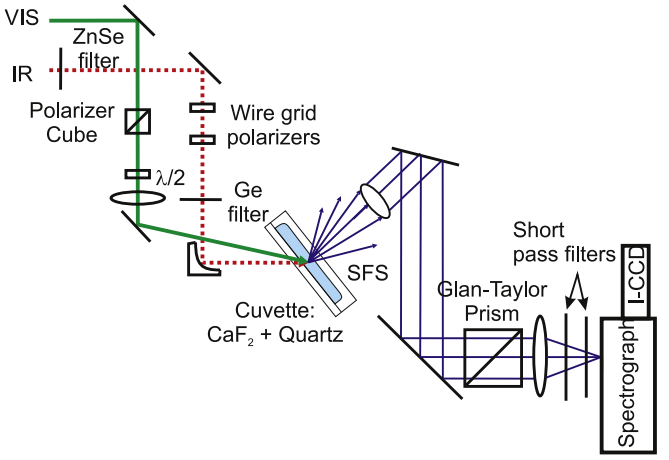

Figure 3. SFS sample stage and detection system. IR (dashed red line) and VIS (green line) are overlapped in the cuvette containing an emulsion. In the focal volume, SF light is generated in a wide angular range which is collimated and steered into the detection system. (For interpretation of references to color in this figure legend, the reader is referred to the web version of this article.)

3. Experimental methods

3.1. Emulsion preparation

To prepare emulsions, we followed a procedure similar to the description in Ref. [29]. 1 vol.% of perdeuterated hexadecane (d-C16) and a D_2O solution, with a known concentration of surfactant, were mixed for 5 min in a 4 mL vial using a hand held homogenizer (TH, OMNI International). The homogenizer consists of a motor driven plastic tip that spins inside a fixed plastic tube. The tip and the tube were immersed in the vial containing the oil and the water and the tip was spun at an angular velocity of 5 RPM. This procedure produced an emulsion with droplets in the micrometer size range which phase separates due to gravity (creams) in a few minutes. To reduce this creaming rate, the droplet size was decreased by placing the vial containing the emulsion in an ultrasound bath (35 kHz, 400 W, Bandelin) for 15 min. Using this method, we could obtain droplets that had an average radius ranging from 50 to 500 nm. The droplets used in this study have an average radius of ~100 nm and a polydispersity index (PDI) of <0.2, as was determined by Dynamic Light Scattering (DLS), using a Malvern ZS nanosizer. The creaming rate for such droplets is 1.3 μm h^{-1}.

All chemicals were used as received. d_{34}-hexadecane (dC16) (98% D) was purchased from Cambridge Isotope. Aqueous solutions were prepared with D_2O (99% D, Aldrich) and sodium dodecylsulfate (SDS) (⩾99%, Alfa Aesar). Glassware was cleaned with 3:7 H_2O_2:H_2SO_4 piranha solution and then thoroughly rinsed with ultra-pure water (0.053 μS/cm, TKA) to remove residual chemicals.

IR spectra were acquired with a Bruker Vertex 70 in the transmission mode, using sample cells with detachable 2.4 mm thick CaF_2 windows.

3.2. The SFS stage

In order to measure scattered sum frequency photons it is necessary to use pulses of ps or fs duration in the mid-IR and VIS frequency range. A thorough description of our laser system can be found in Ref. [30]. Here, we focus only on the details of the SFS setup. Figure 3 depicts a scheme of the SFS sample stage and detection system. The SF scattering experiments are performed using IR pulses (8–12 μJ, ~150 fs, FWHM bandwidth 220 cm^{-1}) spatially and temporally overlapped with 800 nm VIS pulses (8–15 μJ, FWHM bandwidth 5–13 cm^{-1}) in a cuvette containing the emulsion. A 90° off-axis parabolic Au mirror (f = 5 cm) focuses the IR beam down to a ~150 μm beam waist diameter. Two BaF_2 wire grid polarizers control the energy and polarization of the IR beam. The VIS beam polarization is cleaned by a polarizer cube and changed by a $\lambda/2$ plate. The VIS beam is gently focused with a bi-convex lens (f = 50 cm). At the overlapping position, 80% of the VIS beam energy is transmitted through an aperture of 240 μm. The angle between VIS and IR beams is set to 15°, so that the IR beam is still within the boundaries of the VIS beam. In this geometry the volume of overlap is maximum.

The cuvettes (Hellma GmbH, 106 O.20-40, Germany) with various optical path lengths consisted of two detachable windows with one side made out of CaF_2 and the other side made out of quartz. The SF scattered beam was collimated with a 0.5″ diameter plano-convex lens (f = 18 mm, Thorlabs), and directed towards the detection system using two 2″ Ag mirrors. The lens was placed at a scattering angle of 60° with the cuvette exit window (quartz side) oriented parallel to the collimating lens. The polarization of the SF signal was selected with a Glan-Taylor CaF_2 prism. Two short-pass spectral filters (FES750, Thorlabs and 3RD-770, Omega Optical) were placed before the entrance of the spectrometer (Shamrock 303i, Andor Technologies).

The SF signal was spectrally dispersed onto an intensified CCD camera (i-Star DH742, Andor Technologies). The intensifier was triggered by the laser system with a gate time of 8 ns. The acquisition time of a single spectrum was 100–300 s. The presented SF spectra in this study are plotted as a function of IR wavenumber. The y-axis units of all graphs labeled with I_{SF} represent background subtracted data that has been subsequently divided by the VIS and IR input energies (measured before the sample) and acquisition time. Graphs labeled I_{SFS}/I_{IR} represent data that has been divided by a normalized IR pulse. In a typical SF scattering experiment, we measure the SFS spectrum of a reference sample between measurements of the sample of interest.

4. Results and discussion

In the following section we describe the effect of sample cell path length, particle density and IR pulse energy on SF scattering experiments.

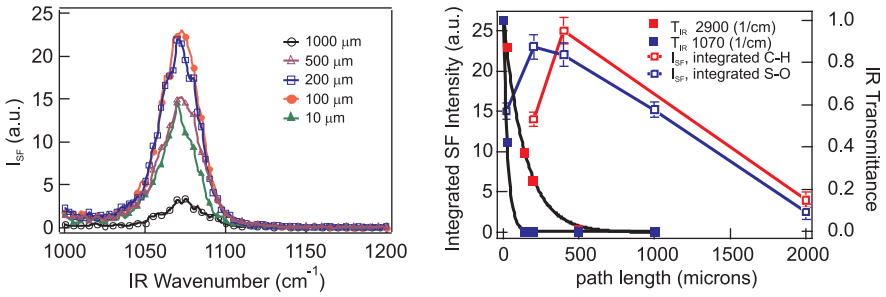

Figure 4. Left: SF scattering spectra in the S–O stretching region taken from a 1 vol.% dC16-in-D_2O emulsion with 8 mM SDS and 100 nm average droplet radius at a scattering angle of $\theta = 60°$ using the *ssp* polarization combination for emulsions using sample cells with different thickness. Right: Integrated intensity as a function of cell thickness. The entire spectral region was used in the integration, i.e., 1025–1125 cm^{-1} for the S–O band and 2800–3000 cm^{-1} for the C–H stretching region. The IR intensity transmitted through a sample cell with different thickness is also shown.

4.1. Path length effects

Starting with the path length dependence, we measured the SF scattered intensity at $\theta = 60°$ using sample cells with different thicknesses. Spectra taken in ssp polarization in the S–O stretching region of the IR spectrum display a single resonant feature at $\sim$ 1075 cm^{-1} and are shown in the left panel of Figure 4. It can be seen that for this spectral region there is an optimal path length of $\sim$100 μm. Increasing the path length further results in a smaller intensity.

The right panel of Figure 4 shows the integrated intensities for the S–O stretch mode (open blue squares). The integrated intensity for spectra recorded in the C–H region are also shown (red closed squares). Note that we have plotted the path length on the *x*-axis, which is given by cell length/cos (θ), with $\theta = 60°$. Also plotted are the transmitted intensities for IR beams at the center frequencies for different path lengths for both spectral regions.

It can be seen that for both modes there is a different path length dependence. The graph shows that the optimum path length coincides with the extinction depth of the IR pulse. This is in agreement with our earlier description. It also shows that the SF photons are generated in a volume rather than on a plane. If the generation of SF photons would take place on a plane, the path length dependence would be very different and would not be varying with IR frequency. The decrease in intensity that occurs at longer path length is not captured by our model, and most likely originates from linear scattering and multiple scattering events of the generated visible and IR beams. As the used droplet densities are typically one order of magnitude larger than the threshold for multiple light scattering (see [28]) this is not surprising. As the limiting process in our experiments is extinction of the IR pulse, our basic model captures the essence of the observed behavior.

4.2. Particle density

Figure 5 shows the signal strength as a function of particle density, measured in a cuvette with a thickness of 100 μm. The integrated intensity of the collected spectra display a linear dependence on the particle density in the sample. Such a dependence has also been observed for second harmonic scattering [8,31]. The intensities of the individual particles are additive because there is no phase relationship between the individual particles. This shows that the process we measure is indeed a scattering process.

Schneider et al. [9] measured the intensity dependence on particle density with SH scattering. Using a sample cell with a path length of 2 mm they observed a linear dependence for malachite green covered polystyrene beads with a diameter of 202 nm up to particles densities of $\sim 40 \times 10^{10}$ particles/ml. At higher densities the intensity decreases. This decrease can be explained by

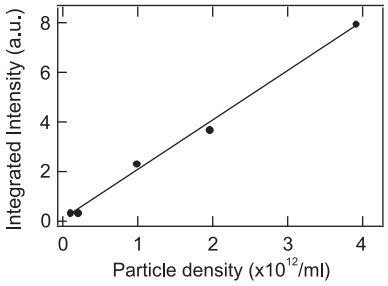

Figure 5. Integrated intensity as a function of droplet density in the sample. The line represents a linear fit. The detection angle is $\theta = 60°$. The SF data was taken from a 1 vol.% dC16-in-D_2O emulsion with 8 mM SDS and 100 nm average droplet radius. The IR frequency was set to the S–O stretch region, the polarization combination was *ppp* and the sample cell path length was 100 μm.

the occurrence of multiple light scattering. The linear increase of our signal indicates that there are no multiple light scattering effects that need to be taken into account.

That particle densities are allowed to be a factor of $\sim$10 higher for SF scattering than for SH scattering is caused by the size of the pulse overlap volume and the interaction of the D_2O solution with the IR pulses, which limits the volume of the sample in which signal is generated in SFS. Comparing now SHS and SFS we see that while in SHS the entire focus volume of the VIS beam can be used to generate SH photons, in SFS this volume is limited by the overlap of two different beams and the extinction of the IR by the bulk liquid. As a consequence the path length for SFS is limited by IR absorbance of the D_2O. This can, however, be compensated by increasing the particle density. For bigger particles this density dependence will be different, however, as the scattering efficiency per particle will be different. Another important variable is the difference in refractive index. A larger contrast between the refractive index of the particles and bulk medium results in a larger scattering cross section. Since the refractive index contrast for SHS of polystyrene particles in water is greater than the refractive index contrast for SFS of oil droplets in water, multiple scattering will occur at lower particle densities for SHS than SFS if all other parameters (size, sample volume, path length) are identical. For SHS, an excellent description of these effects can be found in Refs. [9,7].

4.3. Dependence on IR pulse energy

As the IR pulse energy is at resonance with the molecules in the bulk liquid it needs to be asserted that the incoming pulses are not affecting the sample. Effects caused by the pulses could be laser induced damage or heating [32,33], or laser induced movement of colloids towards a focal point induced by depletion forces that

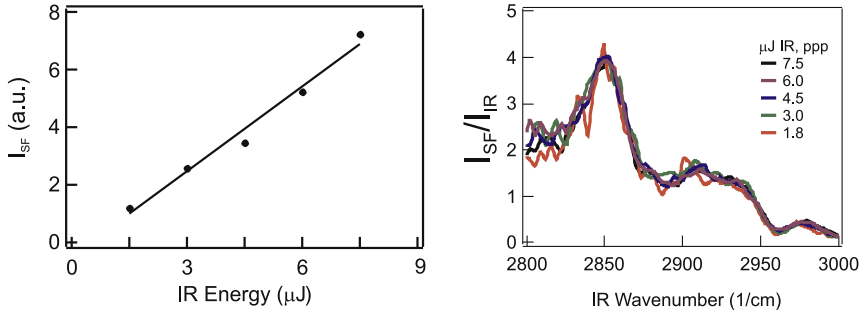

Figure 6. Left: Integrated signal as a function of IR pulse energy. Right: Normalized SF scattering spectra for different IR pulse energies showing no dependence of the spectral shape on IR intensity. The data was taken from a 1 vol.% dC16-in-D_2O emulsion with 8 mM SDS and 100 nm average droplet radius. The polarization combination was *ppp*.

originate from temperature dependent gradients in a (polymer) solution [34].

Although these effects typically occur at higher pulse energies, we measured three markers for stability: the dependence of the overall intensity on input energy, the spectral shape of the signal as a function of IR energy and the signal as a function of time. Measured continuously over a time span if eight hours, the signal is constant in time. The result is shown in Figure 6. The left panel displays the integrated intensity as a function of IR energy. As can be seen, there is a linear relation between intensity and IR intensity, as would be expected for sum frequency generation. The right panel shows the normalized spectra for *ppp* polarization. As can be seen the spectral shape does not change with increasing IR power. Both graphs indicate that there is no induced damage, heating or concentration gradients across the focus. If such effects were present, one would expect to see either a difference in the spectrum or a nonlinear intensity dependence.

5. Conclusions

We have described in detail various aspects of sum frequency scattering. The scattered signal was further quantified by measurements with different optical path lengths. We have shown that for different IR excitation wavelengths a different optimum experimental geometry exists. The optimum optical path length matches roughly the 1/e absorbance length in D_2O of the used IR frequency. For the optimum optical path length, the intensity depends linearly on the particle density. The intensity also scales linearly with the IR pulse energy whereas no changes are observed in the spectral shape.

That the signal to noise ratio (as e.g. in Figure 4, 6) is comparable or greater than sum frequency generation experiments on planar substrates (in e.g. [35]) shows that it is possible to study interfacial processes in three dimensions in aqueous solutions. This allows for the in situ and label-free study of many systems and processes relevant in physical, chemical and biological processes in industry, biology and medicine.

Acknowledgements

We thank R. Scheu for insightful discussions. This work is part of the Research Programme of the Max-Planck Society. We thank the German Science Foundation (Grant No. 560398) and the European Research Council (Startup Grant No. 240556).

References

[1] R.J. Hunter, Found. Colloid Sci. (2002).
[2] J.D. McClements, Crit. Rev. Food. Sci. Tech. 47 (2007) 611.
[3] J. Goodwin, Colloids and Interfaces with Surfactants and Polymers, John Wiley and sons, New York, 2004.
[4] K.B. Eisenthal, Chem. Rev. 106 (4) (2006) 1462.
[5] S. Roke, Chem. Phys. Chem. 10 (2009) 1380.
[6] E.C.Y. Yan, Y. Liu, K.B. Eisenthal, J. Phys. Chem. B 102 (1998) 6331.
[7] B. Schürer, S. Wunderlich, C. Sauerbeck, U. Peschel, W. Peukert, Phys. Rev. B 82 (24) (2010) 241404.
[8] H. Wang, E.C.Y. Yan, E. Borguet, K.B. Eisenthal, Chem. Phys. Lett. 259 (1-2) (1996) 15.
[9] L. Schneider, H.J. Schmid, W. Peukert, Appl. Phys. B 87 (2) (2007) 333.
[10] S.H. Jen, H.L. Dai, J. Phys. Chem. B 110 (46) (2006) 23000.
[11] S.H. Jen, G. Gonella, H.L. Dai, J. Phys. Chem. A 113 (16) (2009) 4758.
[12] M. Subir, J. Liu, K.B. Eisenthal, J. Phys. Chem. C 112 (2008) 15809.
[13] X.M. Shang, Y. Liu, E. Yan, K.B. Eisenthal, J. Phys. Chem. B 105 (51) (2001) 12816.
[14] J. Liu, M. Subir, K. Nguyen, K.B. Eisenthal, J. Phys. Chem. B 112 (2008) 15263.
[15] S. Roke, W.G. Roeterdink, J.E.G.J. Wijnhoven, A.V. Petukhov, A.W. Kleyn, M. Bonn, Phys. Rev. Lett. 91 (2003) 258302.
[16] S. Roke, J. Buitenhuis, J.C. van Miltenburg, M. Bonn, A. van Blaaderen, J. Phys. Condens.Matter 17 (45) (2005) S3469.
[17] S. Roke, O. Berg, J. Buitenhuis, A. van Blaaderen, M. Bonn, Proc. Natl. Acad. Sci. 103 (36) (2006) 13310.
[18] A.G.F. de Beer, H.B. de Aguiar, J.W.F. Nijsen, S. Roke, Phys. Rev. Lett. 102 (2009) 095502-1.
[19] H.B. de Aguiar, A.G.F. de Beer, M.L. Strader, S. Roke, J. Am. Chem. Soc. 132 (2010) 2122, doi:10.1021/ja9095158.
[20] H.B. de Aguiar, M.L. Strader, A.G.F. de Beer, S. Roke, J. Phys. Chem. B 115 (2011) 2970.
[21] M.L. Strader, H.B. de Aguiar, A.G.F. de Beer, S. Roke, Soft Matter 7 (2011) 4959.
[22] S. Roke, M. Bonn, A.V. Petukhov, Phys. Rev. B 70 (2004) 115106-1.
[23] J.I. Dadap, H.B. de Aguiar, S. Roke, J. Chem. Phys. 130 (2009) 214710-1.
[24] S. Jen, H. Dai, G. Gonella, J. Phys. Chem. C 114 (10) (2010) 4302.
[25] A.G.F. de Beer, S. Roke, J. Chem. Phys. 132 (2010) 234702-1.
[26] J. Shan, J.I. Dadap, I. Stiopkin, G.A. Reider, T.F. Heinz, Phys. Rev. A 73 (2) (2006) 023819.
[27] A.G.F. de Beer, S. Roke, Phys. Rev. B 79 (2009) 155420-1.
[28] H.C. van de Hulst, Light Scattering by Small Particles, John Wiley and sons, New York, 1957.
[29] M. Prez, N. Zambrano, M. Ramirez, E. Tyrode, J.L. Salager, J. Dispersion Sci. Technol. 23 (2002) 55.
[30] A.B. Sugiharto, C.M. Johnson, H.B. de Aguiar, L. Aloatti, S. Roke, Appl. Phys. B 91 (2008) 315.
[31] S. Viarbitskaya, V. Kapshai, P. van der Meulen, T. Hansson, Phys. Rev. A 81 (5) (2010) 053850.
[32] B.D. Casson, R. Braun, C.D. Bain, Faraday Discuss. 104 (1996) 209.
[33] J. Hobley, Y. Kuge, S. Gorelik, M. Kasuya, K. Hatanaka, S. Kajimoto, H. Fukumura, Phys. Chem. Chem. Phys. 10 (2008) 5256, doi:10.1039/B805838E.
[34] H.-R. Jiang, H. Wada, N. Yoshinaga, M. Sano, Phys. Rev. Lett. 102 (2009) 208301.
[35] S. Roke, J.M. Schins, M. Müller, M. Bonn, Phys. Rev. Lett. 90 (2003) 128101.